Secreted chemokines and transcriptomic analyses reveal diverse inflammatory and degenerative processes in the intervertebral disc of the STZ-HFD mouse model of Type 2 diabetes

Christian E. Gonzalez[1], Rachana S. Vaidya[2], Sade W. Clayton[2], Simon Y. Tang[1-4]

[1]Department of Biomedical Engineering, Washington University in St. Louis, St. Louis, MO

[2]Department of Orthopaedic Surgery, Washington University School of Medicine, St. Louis, MO

[3]Institute of Material Science and Engineering, Washington University in St. Louis, St. Louis, MO

[4]Department of Mechanical Engineering and Materials Science, Washington University in St. Louis, St. Louis, MO

Corresponding Author:

Simon Y. Tang, Ph.D., MSCI

Associate Professor

Orthopedic Surgery, Biomedical Engineering,

Mechanical Engineering & Materials Science

Washington University in St. Louis

simon.tang@wustl.edu

Keywords: type 2 diabetes; intervertebral disc degeneration; streptozotocin-high-fat-diet; leptin receptor deficiency; chronic inflammatory cytokines

Abstract

The chronic inflammation resultant from type 2 diabetes (T2D) is also associated with spinal pathologies, including intervertebral disc (IVD) degeneration and chronic neck and back pain. Although confounding factors, such as increased weight gain in obesity, studies have shown that even after adjusting age, body mass index, and genetics (e.g. twins), patients with T2D suffer from disproportionately more IVD degeneration and back pain. We hypothesize that chronic T2D fosters a proinflammatory microenvironment within the IVD that promotes degeneration and disrupts disc homeostasis. To test this hypothesis, we evaluated two commonly used mouse models of T2D – the leptin-receptor deficient mouse (db/db) and the chronic high-fat diet in mice with impaired beta-cell function (STZ-HFD). STZ-HFD IVDs were more degenerated and showed differential expression of chemokines from the db/db models. Moreover, the RNAseq analysis revealed vast transcriptional dysregulation of many pathways in the STZ-HFD but not in the db/db tissues. Leptin signaling may be essential to mediating the inflammation in T2D. Taken together, the STZ-HFD may better recapitulates the complexities of the chronic inflammatory processes in the IVD during T2D.

Introduction

{Figure 1}

Type 2 diabetes (T2D) is a prevalent metabolic disorder marked by insulin resistance and prolonged hyperglycemia, impacting millions around the globe and leading to significant healthcare expenses (Srinivasan and Ramarao, 2007; Boucher et al., 2014; Petersen and Shulman, 2018; United States, Center for Disease Control, 2022). This disease shares several characteristics with autoimmune disorders, including the chronic, systemic overexpression of immunomodulating cytokines, which can gradually lead to widespread accrual of tissue damage across multiple organ systems (Itariu and Stulnig, 2014; Chen et al., 2017; de Candia et al., 2019; Daryabor et al., 2020). Among these complications, IVD degeneration is a comorbidity of particular interest due to its chronic-inflammatory etiology (Risbud and Shapiro, 2014; Molinos et al., 2015; Navone et al., 2017; Lyu et al., 2021; Pinto et al., 2023). Additionally, there is a strong association between low back pain and chronic T2D (Robinson et al., 1998; Jhawar et al., 2006; Sakellaridis, 2006; Liu et al., 2018; Alpantaki et al., 2019; Cannata et al., 2019; Broz et al., 2021). Chronic inflammation in T2D, driven by a persistent milieu of chemokines may foster a pro-degenerative microenvironment within the IVD, potentially linking T2D-induced inflammation to accelerated IVD degeneration. While chronic inflammation connects T2D and disc degeneration, the underlying mechanism driving this connection is not well known.

Animal models are essential for studying T2D's impact on IVD degeneration. The db/db mouse model, which harbors a point mutation in the gene encoding for the leptin receptor (Chen et al., 1996; Lee et al., 1996), is widely used to study T2D-related metabolic dysfunctions (Wang et al., 2014). Despite exhibiting many human T2D-like traits—including severe obesity, hyperglycemia, and insulin resistance—its leptin receptor deficiency differs from the

multifactorial etiology of human T2D. In spine research, db/db mice show signs of IVD degeneration, such as increased cell apoptosis and extracellular matrix degradation (Li et al., 2020; Natelson et al., 2020; Lintz et al., 2022). However, the lack of leptin signaling could confound interpretations of disc degeneration, since leptin appears to promote anabolic processes and reduce catabolic activities in IVD cells (Francisco et al., 2018; Gruber et al., 2007; Li et al., 2013; Han et al., 2018; Sharma, 2018; Segar et al., 2019; Curic, 2021).

In contrast, the Streptozotocin-High Fat Diet (STZ-HFD) model offers a non-genic approach to replicating T2D. It induces the condition through pro-glycemic diet and low-dose streptozotocin-induced pancreatic beta-cell dysfunction, avoiding the genetic ablation of systemically impactful hormonal pathways like leptin (as seen in the db/db model) [**Fig. 1A**]. This model is characterized by significant metabolic disturbances to glycemic status, insulin resistance, and body weight, mirroring the human T2D phenotype more closely (Kusakabe et al., 2009; Islam and Wilson, 2012). Additional metabolic characteristics reported in STZ-HFD mouse studies include elevated serum insulin levels, dyslipidemia (increased triglycerides, LDL cholesterol, and total cholesterol), and increased markers of inflammation and oxidative stress (Gilbert et al., 2011; Alquier and Poitout, 2018; Yin et al., 2020). This sets this mouse model apart as valuable tool for studying the complex interactions within diabetic complications without the confounding factor of complete leptin signaling ablation (Kusakabe et al., 2009). Previously this model has been employed in studying diabetic complications in bone (Eckhardt et al., 2020). Our study aims to uncover the mechanisms behind inflammatory-pathway contribution to IVD degeneration and dysfunction, advancing the field's understanding of T2D-related IVD complications.

Inflammatory cytokines are pivotal in both IVD degeneration and T2D, mediating acute

inflammatory responses while perpetuating chronic inflammation and tissue degradation (Guest et al., 2008; Velikova et al., 2021). They regulate key proteins such as ADAMTs and MMPs, driving the degradation of the IVD's extracellular matrix (Bond et al., 1998; Malemud, 2019). The identification and characterization of these cytokines in T2D can highlight new therapeutic targets and early intervention markers (Al-Shukaili et al., 2013; Herder et al., 2013). In the spine, inflammatory cytokines contribute to the breakdown of IVD tissue and the development of pain (Shamji et al., 2010; Risbud and Shapiro, 2014). Pro-inflammatory cytokines like TNF-α, IL-1β, and IL-6 are upregulated in degenerated and herniated disc tissues, exacerbating the inflammatory response and advancing tissue damage (Wuertz and Haglund, 2013; Molinos et al., 2015; Navone et al., 2017; De Geer, 2018). These cytokines also influence the expression of matrix-degrading enzymes such as ADAMTS-4 and MMP-9, thereby accelerating disc degeneration (Tian et al., 2013; Zhang et al., 2015). Their role in T2D is similarly significant, contributing to insulin resistance and beta-cell dysfunction (Calle and Fernandez, 2012). Elevated levels of pro-inflammatory cytokines in patients with T2D underline their importance in disease progression (Guest et al., 2008; Velikova et al., 2021), and targeting these cytokines could open novel therapeutic avenues for both T2D and IVD degeneration (Al-Shukaili et al., 2013; Herder et al., 2013).

This study aims to compare IVD health in db/db and STZ-HFD mouse models of T2D, focusing on inflammation, transcriptomics, and morphological as well as mechanical changes during tissue degeneration [**Figure 1C**] to better understand pathways through which T2D exacerbates IVD degeneration. Our findings will enhance the understanding of the interplay between T2D and IVD homeostasis and demonstrate validity of the STZ-HFD model in recapitulating discogenic changes observed in patients with T2D.

Materials & Methods

Animals.

We used skeletally-mature (12-week-old) male C57BL/6 mice (N = 20) for their established susceptibility to T2D when exposed to a high-fat diet (HFD) and treated with streptozotocin (STZ). Previous findings have indicated that this strain, particularly males, exhibits rapid obesity development under HFD and pronounced insulin resistance following STZ administration (Luo et al., 1998; Mu et al., 2006; Mu et al., 2009). As a result of estrogen-mediated mechanisms of protection, female STZ-HFD mice are resistant to developing T2D and are thus excluded from this study (Medrikova et al., 2012; Pettersson et al., 2012; Stubbins et al., 2012). To contrast the STZ-HFD model's pathology with a well-characterized model of chronic T2D, we included a parallel cohort of 3-month-old homozygous (db/db) male $Lepr^{db}$ mutant mice (n=9) with heterozygous (db/+) littermate controls (n=9), since at this timepoint they have endured a similar duration of T2D symptoms as the STZ-HFD mice. All mice were group-housed (max. 5 mice per cage) under pathogen-free conditions in standard cages; the environment was controlled with a stable temperature and a 12-hour light/dark cycle, with *ad libitum* access to food and water. All procedures were approved by the Institutional Animal Care and Use Committee (IACUC) of Washington University in St. Louis. Regular health and welfare assessments were conducted, including general monitoring of weight, food supply, and behavior.

Study Design.

The study was organized into two phases **[Fig. 1B]**. During the lead-in phase (phase 1), mice were maintained on a HFD for four to six weeks, after which they received a one-time dose of STZ. Following injection, mice continued on the HFD for an additional 12 weeks during the

experimental phase (phase 2). The STZ-HFD group (n = 13) was given a high-fat diet (Research Diets, Inc., D12492i, 60% kcal from fat) for the duration of the study, with the Control + Vehicle group (n = 7) receiving standard mouse chow (5053 PicoLab® Rodent Diet 20, 13% kcal from fat). At the end of the initial phase, baseline measurements of body weight and fasting blood glucose were collected. Following the first phase, STZ-HFD mice were injected intraperitoneally with 100 mg/kg Streptozotocin (MilliporeSigma) in 50 mM sodium citrate buffer (pH 4.5), with Con+Veh animals receiving the sodium citrate buffer only. The two experimental groups received their respective diets for 12 weeks following the injection (experimental phase), and animals were assessed for diabetic status via glucose tolerance. Finally, animals were euthanized, and sterile coccygeal functional spine units (FSUs) including IVDs were harvested from each animal for organ culture and terminal measurements.

Measures of diabetic status.

Several measures of diabetic status were collected at various points throughout the experimental phase, including fasting blood glucose, % A1C, and glucose tolerance **[Fig. 1A]**. Blood glucose levels (mg/dL) were measured using a glucometer (GLUCOCARD Vital® Blood Glucose Meter). Blood samples were drawn via superficial incision to the tail tip of fasted mice using a scalpel; the tail was immediately treated with analgesic (Kwik Stop® Styptic Powder) after blood collection. The percentage of glycated hemoglobin (% A1C) was measured using the A1CNow®+ system (PTS Diagnostics) according to kit instructions. Blood samples were drawn in the same way as during the blood glucose test. Finally, to assess glucose tolerance (glucose tolerance test, GTT), mice were fasted and had their blood glucose measured as described above to establish a baseline. Mice were then injected intraperitoneally with 2 g/kg glucose in sterile

water. Additional blood glucose measurements were taken at 30 min., 60 min., and 90 min. post injection. The area-under-the-curve (AUC) of blood glucose (mg•h/dL) was calculated over the course of the test. For the purpose of evaluating diabetic status for inclusion in the study, a cutoff of 435 mg•h/dL on the GTT, established in previous studies on human T2D criteria (Sakaguchi et al., 2015), was adjusted for time and interspecies differences in blood glucose levels.

Organ culture.

Following extraction, FSUs were cultured in 2 mL Dulbecco's Modified Eagle Medium/Nutrient Mixture F-12 Ham with L-glutamine and 15 mM HEPES (Sigma-Aldrich, D6421). Culture medium was supplemented with 20% fetal bovine serum (Gibco No. A5256801) and 1% penicillin-streptomycin (Gibco No. 15140122). Cultures underwent a preconditioning period of 7 days with regular media changes to account for the inflammatory response from extraction (Fig. 1C). Conditioned media was collected 48 hours after the final media change at the end of the preconditioning period and immediately frozen in -80° C.

Chemokine assay.

A multiplex assay of remodeling factors and inflammatory chemokines (45-Plex Mouse Cytokine Discovery Assay, Eve Technologies Assays; CCL-2,3,4,5,11,12,17,20,21,22; CSF-1,2,3; IL-1α,1β,2,3,4,5,6,7,9,10,11,12A,12B,13,15,16,17; CXCL1,2,5,9,10; CX3CL1; IFN-γ,β1; TNFα; LIF; VEGF; EPO; TIMP-1) was performed on conditioned media samples. Cytokine levels were analyzed using Welch's t-Test. Cytokines with greater than 25% missingness (values outside of assay range) across all experimental groups were excluded from further analysis. Significantly upregulated cytokines in each model were selected for a secondary fold change

analysis, where protein expression levels for db/db and STZ-HFD mice were used to calculate fold change for each cytokine over the corresponding average expression of the control (db/+ and Con+Veh respectively).

Cytokine Interaction Network Construction and Analysis.

To further investigate the inflammatory profiles of these T2D models, networks of cytokine interactions were constructed and analyzed using a custom MATLAB (Version: 9.13.0.2080170 R2022b) script. Networks were generated by calculating a Pearson correlation matrix for each experimental group based on cytokine expression data from the multiplex panel of conditioned media. To interrogate the strong protein correlations, a threshold ($|r| > 0.7$) was applied to the correlation matrices. The filtered matrices were used to create undirected graphs, with nodes representing cytokines and edges representing significant interactions. Centrality measures were calculated to determine the importance of each cytokine within the networks. Eigenvector centrality and betweenness centrality were computed for each network using the centrality function. The resulting centrality values were organized into tables and sorted to identify the top-ranking cytokines. For each centrality metric, shared high-ranking cytokines between the diabetic models and unique cytokines for each diabetic model were aggregated. Additionally, key network characteristics were extracted to understand the structure and function of the cytokine networks. The average path length was determined using the distances function to compute the shortest finite paths between all pairs of nodes. Modularity and community structure were assessed using the Louvain community structure and modularity algorithm (Blondel et al., 2008). We also computed k-hop reachability to assess the extent to which cytokines can influence each other within one (k=1) or two (k=2) steps. The Jaccard index was used to compare the

reachability matrices between different groups, providing a measure of similarity. Finally, the networks were visualized using force-directed layouts with nodes colored by eigenvector centrality and sized by betweenness centrality.

***Histology*.**

Following removal from culture, FSUs were fixed in 10% neutral-buffered formalin (Epredia™ 5735) overnight and decalcified in ImmunoCal (StatLab STL14141) for 72 hours. Samples were fixed in paraffin, sectioned in the sagittal plane at 10 µm thickness, and stained with Safranin-O/Fast Green prior to being imaged via Hamamatsu NanoZoomer with a 20x objective. Blinded histological images of the IVDs were evaluated for degeneration based on a standardized histopathological scoring system (Melgoza et al., 2021).

Contrast-enhanced Micro-computed Tomography.

Functional spine units were incubated in a 175 mg/mL Ioversol solution (OptiRay 350; Guerbet, St. Louis) diluted in PBS at 37 °C. Following 4 hours of incubation, the samples underwent scanning with a Viva CT40 (Scanco Medical) at a 10-µm voxel size, using 45 kVp, 177 µA, high resolution, and a 300 ms integration time. CEµCT data was exported as a DICOM file for analysis in a custom MATLAB program (https://github.com/WashUMusculoskeletalCore/Washington-University-Musculoskeletal-Image-Analyses). After an initial Gaussian filter (kernel size = 5), functional spine units were segmented by drawing a contour around the perimeter of the IVD every 10 transverse slices and morphing using linear interpolation. This was defined as the whole disc mask. The NP was segmented from the whole disc by thresholding and performing morphological close and

morphological open operations to fill interior holes and smooth NP boundaries. The volumes and intensities were calculated from the NP and whole disc regions. Disc height index (DHI) was measured by averaging the height-to-width ratio of the IVD over five slices in the mid-sagittal plane. Finally, the NP intensity/disc intensity (NI/DI) ratio and NP volume fraction (NPVF; NP volume / total volume) was computed using the intensity and volume metrics reported by the output analysis within the MATLAB program. All thresholding and analysis were performed using blinded and validated methods (Lin et al., 2016; Lin and Tang, 2017).

Mechanical Testing.

Mechanical testing of functional spine units was performed using cyclic compression on a microindentation system (BioDent; Active Life Scientific) with a 2.39 mm probe as previously described (Liu et al., 2015). Samples were adhered to an aluminum plate and placed in a PBS bath prior to aligning the sample beneath the probe with a 0.03 N preload. Each unit was then sinusoidally loaded in compression at 1 Hz for 20 cycles with a 35 μm amplitude. A loading slope value was calculated from the linear region of the force-displacement curve, and the loss tangent (tan delta) was calculated from the phase delay between loading and displacement (Liu et al., 2015).

Matrix Protein Assays.

Whole extracted discs were used to measure the biochemical content of various matrix proteins. First, discs were digested overnight in a papain digestion buffer, after which the buffer was collected for a 1,9-dimethylmethylene blue assay of sulfated glycosaminoglycan content with a chondroitin sulfate standard (Liu et al., 2017). The disc was then subjected to high temperature

bulk hydrolyzation in 12 N HCl. Hydrolysates were desiccated and reconstituted with 0.1x phosphate-buffered saline (PBS) and measured against a quinine standard for advanced glycation end product content (Liu et al., 2017). Finally, a hydroxyproline assay was used to quantify collagen content (Liu et al., 2017).

RNA Collection and Sequencing Analysis.

Sterile extracted IVDs were placed directly into cold media. After extraction, IVDs were flash-frozen in liquid nitrogen and homogenized via ball mill (Sartorius Mikro-Dismembrator U). Homogenates were resuspended in TRIzol Reagent (Invitrogen 15596-026) and centrifuged at 800 RCF for 5 minutes. Supernatant was collected, purified, and isolated using column filtration (Zymo Research Direct-zol RNA Microprep Kit R2060). Samples were prepared, indexed, pooled, and sequenced on an Illumina NovaSeq X Plus, with basecalls and demultiplexing done using DRAGEN and BCLconvert version 4.2.4. RNA-seq reads were aligned to the Ensembl release 101 assembly with STAR 2.7.9a1, and gene counts were derived using Subread:featureCount version 2.0.32. Isoform expression was quantified with Salmon 1.5.23, while sequencing performance was assessed using RSeQC 4.04. Gene counts were normalized using EdgeR, and low-expressed genes were excluded. The count matrix was transformed to moderated log 2 counts-per-million with Limma's voomWithQualityWeights, and differential expression analysis was performed. Specific genes related to sugar reduction and dicarbonyl-compound formation (a precursor reaction in the formation of AGEs) were initially identified, along with ligands for RAGE, regulators of NF-kappaB function, and adipokines. A subsequent broader analysis of global perturbations in GO terms, MSigDb, and KEGG pathways was performed using GAGE. To better understand the types of the pathways altered in T2D, pathway

analysis was grouped into functional categories for visualization. For shared or similar pathways within each category, the broader pathway encompassing more genes was elected for visualization. All pathways and genes were filtered for significance with corrections for false-discovery rate, and individual genes were excluded if the absolute value of $\log_2$ (fold change) was less than 1. All visualization was performed using GraphPad Prism 10.3.1 v509. The data discussed in this publication have been deposited in NCBI's Gene Expression Omnibus (Edgar, 2002) and are accessible through GEO Series accession number GSE288503 (https://www.ncbi.nlm.nih.gov/geo/query/acc.cgi?acc=GSE288503).

Results

{Figure 2}

The db/db and STZ-HFD Mouse Models Exhibit a Characteristically Diabetic Phenotype

Both db/db and STZ-HFD mice demonstrate hallmark features of diabetes **[Fig. 2]**. Both groups exhibit AUC GTT values above the defined threshold, indicating impaired glucose tolerance [**Fig. 2A**]. The STZ-HFD mice show severe glucose intolerance compared to Con+Veh mice ($p < 0.0001$). The terminal body weights show that db/db mice weigh significantly more than both db/+ and STZ-HFD mice, [**Fig. 2B**]. The terminal fasting blood glucose levels indicate a significant difference only between the STZ-HFD and Con+Veh groups, demonstrating notable fasting hyperglycemia in the STZ-HFD mice, but not in db/db mice [**Fig. 2C**]. HbA1c levels reveal no difference between db/db mice and STZ-HFD mice, but each group significantly differs from their respective controls [**Fig. 2D**]. This indicates that both models exhibit chronic hyperglycemia, confirming their relevance as models of T2D.

{Figure 3}

Histopathological Analysis Reveals IVD Degeneration in STZ-HFD Mice

The IVDs of STZ-HFD mice exhibited more degeneration compared to the IVDs of controls and the db/db mice. **Figure 3** presents a comparison of histological phenotypes across the four groups (db/+, db/db, Con+Veh, and STZ-HFD), showing the range of histopathological scores within this study [**Fig. 3A**]. Histopathological scoring revealed that only the STZ-HFD mice exhibit significantly greater IVD degeneration compared to the control group [**Fig. 3B**]. In the Con+Veh samples, the annulus fibrosus has healthy, convexed outer lamellae (➡) and well-organized, concentric inner lamellae (▼). In contrast, the STZ-HFD samples show degenerate

crimped, concave outer lamellae (⇨) and wavy, disorganized inner lamellae (▽), indicating altered matrix structure in the AF **[Fig. 3C]**.

{Figure 4}

CT Analysis, Matrix Assays, and Mechanical Testing All Show No Major Effects in T2D IVD

The analysis of CEμCT data, mechanical testing, and matrix protein assays revealed only one significant difference among the four groups across all nine measured outcomes. Specifically, parameters such as NI/DI, NPVF, loading slope, hysteresis energy, tan delta, and biochemical content showed no variations between groups. The only statistically significant result was a difference in morphology between the db/db and STZ-HFD groups, as indicated by the DHI. These findings suggest that the structural integrity, mechanical behavior, and biochemical composition of the IVDs are mostly consistent across the db/db and STZ-HFD models. The lack of significant differences broadly implies that, under the conditions tested, type 2 diabetes does not markedly affect IVD properties in these models and cannot further establish the degenerate features gleaned in the histopathological analysis. This highlights the need for more sensitive measures or longer study durations to detect subtle changes related to T2D.

{Figure 5}

Immunomodulatory Cytokines Are Chronically Upregulated in STZ-HFD IVDs

The comparative analysis of cytokine expression levels between db/db and STZ-HFD models provides novel insights into diabetic inflammation of the IVD. The initial comparative analysis of the two models' protein expression levels revealed that two cytokines (CCL2, CCL3) and sixteen cytokines (CCL2,3,4,5,12; CXCL1,2,9,10; CX3CL1; IL-2,6,16; CSF-3; VEGF; LIF)

were upregulated in the db/db and STZ-HFD models respectively, and thus included in the fold change analysis. The fold change in cytokine levels is computed over their respective controls (db/+ for db/db, Con+Veh for STZ-HFD) **[Fig. 4A]**. The STZ-HFD model exhibited a significantly higher fold increase compared to the db/db model for 8 cytokines: CXCL2, CCL2, CCL3, CCL4, CCL12 (monocyte/macrophage associated cytokines) (Sagar et al., 2012; Arendt et al., 2013; Lança et al., 2013; Etna et al., 2014; Motwani and Gilroy, 2015; He et al., 2016; Lim et al., 2016; DeLeon-Pennell et al., 2017; Ruytinx et al., 2018; Sindhu et al., 2019; Zhang et al., 2019, 38; Huang et al., 2020; Pelisch et al., 2020; Yang et al., 2020; Xu et al., 2021a; Xu et al., 2021b; Sheng et al., 2022), IL-2, CXCL9 (T-cell associated cytokines) (Chang and Radbruch, 2007; Venetz et al., 2010; Shachar and Karin, 2013; Ochiai et al., 2015; Boff et al., 2018; Kuo et al., 2018; Mortara et al., 2018; House et al., 2020; Marcovecchio et al., 2021; Markovics et al., 2022), and CCL5 (pleiotropic cytokine) (Juhas et al., 2015; Atri et al., 2018; Kranjc et al., 2019; Chen et al., 2020; Zeng et al., 2022). Representing the overlapping cytokine expression profiles through a Venn diagram revealed that the STZ-HFD model encompassed a large number of upregulated cytokines [**Figure 4B**]. The inner circle represents the db/db model, containing only the two upregulated cytokines, both of which are also upregulated in the STZ-HFD model. This indicates that the STZ-HFD model has a broader and more pronounced cytokine response compared to the db/db model.

{Figure 6}

Differential Network Structures Reveal Unique Inflammatory Pathways of T2D in IVD

Our analysis of cytokine networks in these two models revealed several key insights into the inflammatory pathways associated with T2D (**Fig. 6A**). CCL2 and CCL4 emerged as pivotal

cytokines in both models based on betweenness centrality, highlighting their crucial roles in maintaining network connectivity (**Error! Reference source not found.**). In the db/db mouse model, unique cytokines were identified that are likely influenced by the absence of leptin signaling. These included CSF-3 (betweenness centrality), CXCL-5, CXCL-9, CXCL-10, and IL-4 (eigenvector centrality), and IL-11 (both centralities) (**Error! Reference source not found.**). In contrast, the STZ-HFD mouse model, which maintains functional leptin signaling and mimics human T2D etiology, presented a different profile of unique cytokines. CXCL2 and IL-6 (betweenness centrality), and IL-16, CCL11, and CSF3 (eigenvector centrality) were central in this model (**Error! Reference source not found.**). This indicates that these cytokines may be independently regulated through pathways that are either bypassed or inhibited in the simultaneous presence of leptin signaling and T2D-associated chronic inflammation. The db/db model demonstrated a shorter average path length compared to the STZ-HFD model (**Error! Reference source not found.**), indicating more efficient communication within the cytokine network of the db/db model. The longer path length in the STZ-HFD model suggests a more dispersed network structure, consistent with the wide array of upregulated cytokines across multiple signaling cascades. Additionally, the STZ-HFD network had the highest modularity (**Error! Reference source not found.**). Higher modularity in the STZ-HFD model indicates well-defined communities within the cytokine network, reflecting distinct functional signaling pathways in a broad inflammatory response. The lower modularity in the db/db model suggests a less distinct community structure and a more generic inflammatory response. The Jaccard index values for the STZ-HFD and WT comparisons were 0.144 (k=1) and 0.246 (k=2), indicating low similarity between these networks. Comparisons between db/db and db/+ showed slightly higher values, indicating closer similarity (**Error! Reference source not found.**). This suggests

significant changes in the cytokine networks of the STZ-HFD model, while the db/db model retains more similarity to its control, reflecting less drastic alterations to the inflammatory signaling cascade.

{Figure 7}

STZ-HFD IVDs Show Distinct Gene Expression and Pathway Dysregulation in RNA-Seq Analysis

The RNA-seq analysis revealed significant differences between the db/db and STZ-HFD models in several biological processes, particularly those related to type 2 diabetes-related pathways, immune response, ECM organization, metabolic function, and signal transduction. Seven genes associated with non-enzymatic glycosylation and sugar reduction, both critical processes in Type 2 Diabetes pathology through the formation of AGEs, were differentially expressed between the db/db and STZ-HFD models (**Fig. 7A**). In the db/db model, 2 genes were upregulated and 1 was downregulated (*Cbr3, Aldoa; Pfkp*), whereas in the STZ-HFD model, 4 genes were upregulated and 2 were downregulated (*Tpi1, Aldoa, Pfkfb1, Pfkm; Aldoc, Pfkp*). This indicates a more pronounced alteration in pathways related to formation of advanced glycation end products (AGEs), under STZ=HFD conditions. Additionally, *ITGB2*, a component of an alternative ligand for the receptor for AGEs (RAGE), which play a key role in diabetic complications, was downregulated compared to controls in both models (**Fig. 7A**). Notably, the RAGE receptor itself did not show significant changes in either model. Furthermore, NF-κB signaling, a pathway implicated in inflammatory responses downstream of RAGE signaling, was moderately affected; in the db/db model, one gene was upregulated and one downregulated (*Tank; Nfkbiz*), while only one gene (*Nfkbiz*) was downregulated in the STZ-HFD model (**Fig.**

7A). Regarding adipokine signaling, which is critical in the regulation of glucose and lipid metabolism in Type 2 Diabetes, 2 genes related to leptin signaling (*Lepr, Lep*) were differentially expressed in the STZ-HFD model and not in the db/db model (**Fig. 7A**). This ultimately strengthens our initial hypothesis regarding the role of leptin signaling in mediating diabetic inflammation and degeneration of the IVD.

Enrichment analysis identified eight pathways in the Molecular Signatures Database (MSigDB, https://www.gsea-msigdb.org/gsea/msigdb) significantly affected in the STZ-HFD model, all of which are crucial for immune response and inflammation. These included the upregulation of ubiquitination and proteasome degradation, and the downregulation of pathways such as Fcgamma receptor-dependent phagocytosis, cell surface interactions at the vascular wall, innate immune system, transcriptional regulation of granulopoiesis, the Tyrobp causal network in microglia, complement cascade, and lymphoid/non-lymphoid interactions (**Fig. 7B**). Interestingly, none of these pathways were significantly altered in the db/db model, highlighting a distinct inflammatory and immune regulation in the STZ-HFD model.

Eight MSigDB pathways related to ECM and structural organization were significantly altered between the models. In the db/db model, the pathway associated with cell adhesion molecules was downregulated. Conversely, in the STZ-HFD model, several pathways were downregulated, including amyloid fiber formation, collagen formation, chondroitin sulfate metabolism, proteoglycans, glycosaminoglycan metabolism, ECM glycoproteins, and the matrisome (**Fig. 7C**). This suggests that ECM remodeling and structural integrity are more disrupted under STZ-HFD conditions compared to db/db at the transcriptional level.

The analysis also revealed six MSigDB pathways significantly impacted by metabolic function. Both models showed upregulation in oxidative phosphorylation, TCA cycle and

respiratory electron transport, and fatty acid metabolism. However, additional pathways were specifically upregulated in the STZ-HFD model, including glyoxylate metabolism and glycine degradation, amino acid metabolism, and glycolysis and gluconeogenesis (**Fig. 7D**). This indicates a greater depth to the metabolic dysfunction in the STZ-HFD model relative to db/db.

Finally, six MSigDB pathways were identified as being significantly involved in signal transduction and tissue differentiation. In the STZ-HFD model, pathways related to protein localization and PPAR signaling were upregulated, while pathways involved in secreted factors, the formation of beta-catenin complexes, IGF transport and IGFBP uptake, and endochondral ossification were downregulated (**Fig. 7E**). These findings suggest alterations in signaling mechanisms and tissue differentiation processes that are more pronounced in the STZ-HFD model compared to db/db. Overall, the STZ-HFD model exhibited more extensive and varied disruptions across multiple canonical biological pathways, as well as type 2 diabetes-related genes and processes, including those involved in glycosylation, immune response, ECM structure, metabolism, and signal transduction, indicating its utility in studying complex metabolic and inflammatory disorders compared to the db/db model.

Discussion

This study offers novel insights into the chronic inflammatory profiles and degeneration in the IVD of murine T2D models, specifically comparing the db/db and STZ-HFD mouse models. Our key findings indicate that while both models display characteristic diabetic phenotypes (Dalgaard and Pedersen, 2001; Cefalu, 2006; Lin and Sun, 2010), the STZ-HFD model shows pronounced IVD degeneration and a more extensive inflammatory response, positioning it as a more clinically relevant model for studying T2D-related complications and inflammation in the IVD. (Gilbert et al., 2011; Stott and Marino, 2020).

In terms of IVD degeneration, our study demonstrates that histopathologically STZ-HFD mice exhibit significantly greater IVD degeneration compared to controls, indicating a notable degenerative phenotype. Assessment of structural integrity, mechanical behavior, and biochemical composition did not reveal further significant differences, however. In contrast, db/db mice, despite severe obesity, insulin resistance, and chronic hyperglycemia, show milder IVD degeneration compared to littermate controls. This observation aligns with existing literature which reports moderate IVD degeneration in db/db mice influenced by variables such as sex and specific metabolic disruptions (Lintz et al., 2022; Natelson et al., 2020; Li et al., 2020).

Our findings establish the STZ-HFD model as a superior and more physiologically relevant platform to study T2D associated inflammation. This model demonstrated a pronounced upregulation of 16 different cytokines, including key mediators involved in monocyte and macrophage recruitment, T-cell activation, and pleiotropic immune response. Notably, the upregulation of cytokines such as CXCL2 (Rebuffat et al., 2018; Pan et al., 2021), CCL2, CCL3 (Neumeier et al., 2011; Arner et al., 2012; Sullivan et al., 2013; Sindhu et al., 2017; Chang et al.,

2021), CXCL9, IL2 (Higurashi et al., 2009; Nawaz et al., 2013; Pan et al., 2021; Suri et al., 2022), CCL4 (Chang et al., 2021; Pan et al., 2021; Mir et al., 2024) and CCL5 closely mirrors inflammatory profiles observed in human T2D (Keophiphath et al., 2010; Pettigrew et al., 2010; Inayat et al., 2019; Chang et al., 2021; Pan et al., 2021; Alshammary et al., 2023; Mir et al., 2024), highlighting its translational potential. In contrast, the db/db model, while still relevant, exhibits a more limited cytokine profile, limited by the absence of leptin signaling (Francisco et al., 2018).

Cytokine network analysis further identified the distinct cytokine interactions in STZ-HFD IVD, revealing regulatory mechanisms and broader pathway activation. This model exhibited greater network modularity and longer average path length, suggesting a highly structured and complex inflammatory response involving specific functional pathways, reflecting the interplay between obesity, insulin resistance and systemic inflammation (Francisco et al., 2018; Rebuffat et al., 2018; Sharma, 2018; Segar et al., 2019; Pan et al., 2021). Key cytokines such as CXCL2, IL-6, IL-16, CCL11, and CSF3 emerged as central mediators, indicating their potential as therapeutic targets for attenuating T2D inflammation in the IVD. In contrast, the db/db model and the absence of leptin signaling resulted in a compensatory inflammatory network dominated by cytokines like CSF-3, CXCL-5, CXCL-9, CXCL-10, IL-4, and IL-11. Leptin's role in regulating the immune responses is essential (Francisco et al., 2018); and its deficiency may have resulted in a stifled, less complex inflammatory response, which also aligns with the less severe increase in IVD degeneration over controls

The RNA-seq data reveals significant transcriptional alterations in T2D related pathways within the IVD, underscoring that the IVD is not spared from the metabolic and inflammatory complications of T2D, particularly in the STZ-HFD model. This model showed alterations in

non-enzymatic glycosylation and sugar reduction pathways, indicate a hyperglycemic environment conducive to the formation of AGEs (Twarda-Clapa et al., 2022), and effectively captured early molecular events that lead to AGE accumulation and subsequent tissue damage within the IVD, though the 12 week timepoint may not suffice for AGEs deposition in the IVD matrix. Additionally, changes in leptin, RAGE, and NF-kB pathways indicate the STZ-HFD model's potential for studying chronic inflammation and oxidative stress-related complications within the IVD, a key aspect of T2D pathology (Broz et al., 2021). The lack of significant changes in the RAGE receptor itself, combined with downregulation of RAGE ligands in the STZ-HFD model, suggests a complex inflammatory profile that might be indicative of a chronic rather than acute response within the IVD tissue.

Canonical pathway analysis further emphasizes the distinct biological functions altered in these T2D models. In the STZHFD model, the significant upregulation of ubiquitination and proteasome degradation pathways, coupled with the downregulation of immune-related pathways within the IVD, suggests a stress response aimed at managing protein damage, reflecting the chronic inflammatory state associated with metabolic diseases like T2D (Garcia-Martinez et al., 2015). The downregulation of ECM and structural organization pathways, including collagen formation and ECM glycoproteins, hints at impairment of tissue remodeling and fibrosis within the IVD, aligning with the structural changes observed in the histopathological analysis of the STZHFD IVD. In contrast, metabolic pathways such as oxidative phosphorylation and fatty acid metabolism were upregulated in both models, reflecting increased metabolic demands. However, the STZHFD model showed additional upregulation in pathways like glyoxylate metabolism and glycolysis/gluconeogenesis, indicating more extensive metabolic reprogramming within the IVD, further illustrating the model's ability to capture the systemic nature of T2D-related

complications (Joshi et al., 2020; Dhawan et al., 2022).

The transcriptional data, while revealing, must be interpreted with caution, particularly within the context of IVD tissue. While the STZHFD model showed downregulation of ECM-related pathways at the mRNA level, compensatory translational mechanisms may prevent a corresponding reduction in ECM proteins, and the modest changes in NF-κB signaling underscore the limitations of transcriptomic data alone (Mobeen and Ramachandran, 2020; Wang et al., 2020). Consequently, integrating proteomic data with transcriptomic analyses is essential for fully understanding the molecular underpinnings of T2D in the IVD.

Despite these significant findings, this study has several limitations. The selection of cytokines examined was relatively small, potentially missing other important inflammatory mediators involved in IVD degeneration. Additionally, the mechanistic link between inflammation and degeneration remains unclear and warrants further investigation. While the STZ-HFD model provides a comprehensive inflammatory profile, the specific pathways driving the observed IVD degeneration need to be elucidated through future studies to appropriately identify therapeutic targets. Future directions for research based on our findings include expanding the panel of cytokines and other inflammatory mediators examined in the STZ-HFD model to gain a more complete understanding of the inflammatory landscape in T2D. Investigating the specific molecular and cellular mechanisms linking inflammation to IVD degeneration will be crucial to furthering future therapeutic approaches. Finally, exploring therapeutic interventions targeting the identified cytokine pathways could provide insights into potential treatments for T2D-related IVD degeneration.

In conclusion, our findings establish the STZ-HFD model as a more physiologically relevant model for studying T2D-related inflammation and IVD degeneration. The extensive

cytokine upregulation and significant degenerative phenotype observed in this model provide a valuable framework for future research into T2D-associated pathologies. The db/db model, while still relevant, exhibits a more stunted cytokine profile and limited IVD degeneration, making it less representative of the chronic inflammatory environment seen in human T2D. These insights enhance our understanding of T2D-induced IVD degeneration and identify key cytokine pathways for therapeutic development, emphasizing the need to address these pathways holistically for effective intervention.

Competing Interests

Authors declare no competing interests.

Acknowledgements

This work was supported by the NIH R01AR074441 and P30AR074992. Thank you to the Alafi Neuroimaging Lab for Nanozoomer Access (NIH S10RR027552). Multiplex cytokine panels were performed by Eve Technologies Corp.

References

Alpantaki, K., Kampouroglou, A., Koutserimpas, C., Effraimidis, G. and Hadjipavlou, A. (2019). Diabetes mellitus as a risk factor for intervertebral disc degeneration: a critical review. *Eur. Spine J.* **28**, 2129–2144.

Alquier, T. and Poitout, V. (2018). Considerations and guidelines for mouse metabolic phenotyping in diabetes research. *Diabetologia* **61**, 526–538.

Alshammary, A. F., Alshammari, A. M., Alsobaie, S. F., Alageel, A. A. and Ali Khan, I. (2023). Evidence from genetic studies among rs2107538 variant in the *CCL5* gene and Saudi patients diagnosed with type 2 diabetes mellitus. *Saudi J. Biol. Sci.* **30**, 103658.

An In Vitro Organ Culture Model of the Murine Intervertebral Disc.

Arendt, L. M., McCready, J., Keller, P. J., Baker, D. D., Naber, S. P., Seewaldt, V. and Kuperwasser, C. (2013). Obesity Promotes Breast Cancer by CCL2-Mediated Macrophage Recruitment and Angiogenesis. *Cancer Res.* **73**, 6080–6093.

Atri, C., Guerfali, F. Z. and Laouini, D. (2018). Role of Human Macrophage Polarization in Inflammation during Infectious Diseases. *Int. J. Mol. Sci.* **19**, 1801.

Blondel, V. D., Guillaume, J.-L., Lambiotte, R. and Lefebvre, E. (2008). Fast unfolding of communities in large networks. *J. Stat. Mech. Theory Exp.* **2008**, P10008.

Boff, D., Crijns, H., Janssens, R., Vanheule, V., Menezes, G. B., Macari, S., Silva, T. A., Amaral, F. A. and Proost, P. (2018). The chemokine fragment CXCL9(74–103) diminishes neutrophil recruitment and joint inflammation in antigen-induced arthritis. *J. Leukoc. Biol.* **104**, 413–422.

Boucher, J., Kleinridders, A. and Kahn, C. R. (2014). Insulin Receptor Signaling in Normal and Insulin-Resistant States. *Cold Spring Harb. Perspect. Biol.* **6**, a009191–a009191.

Broz, K., Walk, R. E. and Tang, S. Y. (2021). Complications in the spine associated with type 2 diabetes: The role of advanced glycation end-products. *Med. Nov. Technol. Devices* **11**, 100065.

Cannata, F., Vadalà, G., Ambrosio, L., Fallucca, S., Napoli, N., Papalia, R., Pozzilli, P. and Denaro, V. (2019). Intervertebral disc degeneration: A focus on obesity and type 2 diabetes. *Diabetes Metab. Res. Rev.* **36**,.

Cefalu, W. T. (2006). Animal Models of Type 2 Diabetes: Clinical Presentation and Pathophysiological Relevance to the Human Condition. *ILAR J.* **47**, 186–198.

Chang, H.-D. and Radbruch, A. (2007). The Pro- and Anti-Inflammatory Potential of Interleukin-12. *Ann. N. Y. Acad. Sci.* **1109**, 40–46.

Chang, T.-T., Lin, L.-Y. and Chen, J.-W. (2021). A Novel Resolution of Diabetes: C-C Chemokine Motif Ligand 4 Is a Common Target in Different Types of Diabetes by Protecting Pancreatic Islet Cell and Modulating Inflammation. *Front. Immunol.* **12**,.

Chen, L., Deng, H., Cui, H., Fang, J., Zuo, Z., Deng, J., Li, Y., Wang, X. and Zhao, L. (2017). Inflammatory responses and inflammation-associated diseases in organs. *Oncotarget* **9**, 7204–7218.

Chen, L., Zhang, Q., Yu, C., Wang, F. and Kong, X. (2020). Functional roles of CCL5/RANTES in liver disease. *Liver Res.* **4**, 28–34.

Dalgaard, L. T. and Pedersen, O. (2001). Uncoupling proteins: functional characteristics and role in the pathogenesis of obesity and Type II diabetes. *Diabetologia* **44**, 946–965.

Daryabor, G., Atashzar, M. R., Kabelitz, D., Meri, S. and Kalantar, K. (2020). The Effects of Type 2 Diabetes Mellitus on Organ Metabolism and the Immune System. *Front. Immunol.* **11**,.

de Candia, P., Prattichizzo, F., Garavelli, S., De Rosa, V., Galgani, M., Di Rella, F., Spagnuolo, M. I., Colamatteo, A., Fusco, C., Micillo, T., et al. (2019). Type 2 Diabetes: How Much of an Autoimmune Disease? *Front. Endocrinol.* **10**,.

DeLeon-Pennell, K. Y., Iyer, R. P., Ero, O. K., Cates, C. A., Flynn, E. R., Cannon, P. L., Jung, M., Shannon, D., Garrett, M. R., Buchanan, W., et al. Periodontal-induced chronic inflammation triggers macrophage secretion of Ccl12 to inhibit fibroblast-mediated cardiac wound healing. *JCI Insight* **2**, e94207.

Dhawan, P., Vasishta, S., Balakrishnan, A. and Joshi, M. B. (2022). Mechanistic insights into glucose induced vascular epigenetic reprogramming in type 2 diabetes. *Life Sci.* **298**, 120490.

Eckhardt, B. A., Rowsey, J. L., Thicke, B. S., Fraser, D. G., O'Grady, K. L., Bondar, O. P., Hines, J. M., Singh, R. J., Thoreson, A. R., Rakshit, K., et al. Accelerated osteocyte senescence and skeletal fragility in mice with type 2 diabetes. *JCI Insight* **5**, e135236.

Edgar, R. (2002). Gene Expression Omnibus: NCBI gene expression and hybridization array data repository. *Nucleic Acids Res.* **30**, 207–210.

Etna, M. P., Giacomini, E., Severa, M. and Coccia, E. M. (2014). Pro- and anti-inflammatory cytokines in tuberculosis: A two-edged sword in TB pathogenesis. *Semin. Immunol.* **26**, 543–551.

Francisco, V., Pino, J., Campos-Cabaleiro, V., Ruiz-Fernández, C., Mera, A., Gonzalez-Gay, M. A., Gómez, R. and Gualillo, O. (2018). Obesity, Fat Mass and Immune System: Role for Leptin. *Front. Physiol.* **9**, 640.

Garcia-Martinez, I., Shaker, M. E. and Mehal, W. Z. (2015). Therapeutic Opportunities in Damage-Associated Molecular Pattern-Driven Metabolic Diseases. *Antioxid. Redox Signal.* **23**, 1305–1315.

Gilbert, E. R., Fu, Z. and Liu, D. (2011). Development of a Nongenetic Mouse Model of Type 2 Diabetes. *J. Diabetes Res.* **2011**, 416254.

He, M., Dong, H., Huang, Y., Lu, S., Zhang, S., Qian, Y. and Jin, W. (2016). Astrocyte-Derived CCL2 is Associated with M1 Activation and Recruitment of Cultured Microglial Cells. *Cell. Physiol. Biochem.* **38**, 859–870.

Higurashi, M., Ohya, Y., Joh, K., Muraguchi, M., Nishimura, M., Terawaki, H., Yagui, K., Hashimoto, N., Saito, Y. and Yamada, K. (2009). Increased urinary levels of CXCL5, CXCL8 and CXCL9 in patients with Type 2 diabetic nephropathy. *J. Diabetes Complications* **23**, 178–184.

House, I. G., Savas, P., Lai, J., Chen, A. X. Y., Oliver, A. J., Teo, Z. L., Todd, K. L., Henderson, M. A., Giuffrida, L., Petley, E. V., et al. (2020). Macrophage-Derived CXCL9 and CXCL10 Are Required for Antitumor Immune Responses Following Immune Checkpoint Blockade. *Clin. Cancer Res.* **26**, 487–504.

Huang, J., Yang, G., Xiong, X., Wang, M., Yuan, J., Zhang, Q., Gong, C., Qiu, Z., Meng, Z., Xu, R., et al. (2020). Age-related CCL12 Aggravates Intracerebral Hemorrhage-induced Brain Injury via Recruitment of Macrophages and T Lymphocytes. *Aging Dis.* **11**, 1103–1115.

Inayat, H., Azim, M. K. and Baloch, A. A. (2019). Analysis of Inflammatory Gene Expression Profile of Peripheral Blood Leukocytes in Type 2 Diabetes. *Immunol. Invest.* **48**, 618–631.

Islam, Md. S. and Wilson, R. D. (2012). Experimentally Induced Rodent Models of Type 2 Diabetes. In *Animal Models in Diabetes Research* (ed. Joost, H.-G.), Al-Hasani, H.), and Schürmann, A.), pp. 161–174. Totowa, NJ: Humana Press.

Itariu, B. K. and Stulnig, T. M. (2014). Autoimmune Aspects of Type 2 Diabetes Mellitus - A Mini-Review. *Gerontology* **60**, 189–196.

Jhawar, B. S., Fuchs, C. S., Colditz, G. A. and Stampfer, M. J. (2006). Cardiovascular risk factors for physician-diagnosed lumbar disc herniation. *Spine J.* **6**, 684–691.

Joshi, M. B., Ahamed, R., Hegde, M., Nair, A. S., Ramachandra, L. and Satyamoorthy, K. (2020). Glucose induces metabolic reprogramming in neutrophils during type 2 diabetes to form constitutive extracellular traps and decreased responsiveness to lipopolysaccharides. *Biochim. Biophys. Acta BBA - Mol. Basis Dis.* **1866**, 165940.

Juhas, U., Ryba-Stanisławowska, M., Szargiej, P. and Myśliwska, J. (2015). Different pathways of macrophage activation and polarization. *Postępy Hig. Med. Dośw.* **69**, 496–502.

Keophiphath, M., Rouault, C., Divoux, A., Clément, K. and Lacasa, D. (2010). CCL5 Promotes Macrophage Recruitment and Survival in Human Adipose Tissue. *Arterioscler. Thromb. Vasc. Biol.* **30**, 39–45.

Kranjc, M. K., Novak, M., Pestell, R. G. and Lah, T. T. (2019). Cytokine CCL5 and receptor CCR5 axis in glioblastoma multiforme. *Radiol. Oncol.* **53**, 397–406.

Kuo, P., Tuong, Z. K., Teoh, S. M., Frazer, I. H., Mattarollo, S. R. and Leggatt, G. R. (2018). HPV16E7-Induced Hyperplasia Promotes CXCL9/10 Expression and Induces CXCR3+ T-Cell Migration to Skin. *J. Invest. Dermatol.* **138**, 1348–1359.

Kusakabe, T., Tanioka, H., Ebihara, K., Hirata, M., Miyamoto, L., Miyanaga, F., Hige, H., Aotani, D., Fujisawa, T., Masuzaki, H., et al. (2009). Beneficial effects of leptin on glycaemic and lipid control in a mouse model of type 2 diabetes with increased adiposity induced by streptozotocin and a high-fat diet. *Diabetologia* **52**, 675–683.

Lança, T., Costa, M. F., Gonçalves-Sousa, N., Rei, M., Grosso, A. R., Penido, C. and Silva-Santos, B. (2013). Protective Role of the Inflammatory CCR2/CCL2 Chemokine Pathway through Recruitment of Type 1 Cytotoxic γδ T Lymphocytes to Tumor Beds. *J. Immunol.* **190**, 6673–6680.

Lim, S. Y., Yuzhalin, A. E., Gordon-Weeks, A. N. and Muschel, R. J. (2016). Targeting the CCL2-CCR2 signaling axis in cancer metastasis. *Oncotarget* **7**, 28697–28710.

Lin, Y. and Sun, Z. (2010). Current views on type 2 diabetes. *J. Endocrinol.* **204**, 1.

Lin, K. H. and Tang, S. Y. (2017). The Quantitative Structural and Compositional Analyses of Degenerating Intervertebral Discs Using Magnetic Resonance Imaging and Contrast-Enhanced Micro-Computed Tomography. *Ann. Biomed. Eng.* **45**, 2626–2634.

Lin, K. H., Wu, Q., Leib, D. J. and Tang, S. Y. (2016). A novel technique for the contrast-enhanced microCT imaging of murine intervertebral discs. *J. Mech. Behav. Biomed. Mater.* **63**, 66–74.

Liu, J. W., Abraham, A. C. and Y. Tang, S. (2015). The high-throughput phenotyping of the viscoelastic behavior of whole mouse intervertebral discs using a novel method of dynamic mechanical testing. *J. Biomech.* **48**, 2189–2194.

Liu, X., Pan, F., Ba, Z., Wang, S. and Wu, D. (2018). The potential effect of type 2 diabetes mellitus on lumbar disc degeneration: a retrospective single-center study. *J. Orthop. Surg.* **13**, 52.

Luo, J., Quan, J., Tsai, J., Hobensack, C. K., Sullivan, C., Hector, R. and Reaven, G. M. (1998). Nongenetic mouse models of non—insulin-dependent diabetes mellitus. *Metabolism* **47**, 663–668.

Lyu, F.-J., Cui, H., Pan, H., MC Cheung, K., Cao, X., Iatridis, J. C. and Zheng, Z. (2021). Painful intervertebral disc degeneration and inflammation: from laboratory evidence to clinical interventions. *Bone Res.* **9**, 1–14.

Marcovecchio, P. M., Thomas, G. and Salek-Ardakani, S. (2021). CXCL9-expressing tumor-associated macrophages: new players in the fight against cancer. *J. Immunother. Cancer* **9**, e002045.

Markovics, A., Rosenthal, K. S., Mikecz, K., Carambula, R. E., Ciemielewski, J. C. and Zimmerman, D. H. (2022). Restoring the Balance between Pro-Inflammatory and Anti-Inflammatory Cytokines in the Treatment of Rheumatoid Arthritis: New Insights from Animal Models. *Biomedicines* **10**, 44.

Medrikova, D., Jilkova, Z. M., Bardova, K., Janovska, P., Rossmeisl, M. and Kopecky, J. (2012). Sex differences during the course of diet-induced obesity in mice: adipose tissue expandability and glycemic control. *Int. J. Obes.* **36**, 262–272.

Melgoza, I. P., Chenna, S. S., Tessier, S., Zhang, Y., Tang, S. Y., Ohnishi, T., Novais, E. J., Kerr, G. J., Mohanty, S., Tam, V., et al. (2021). Development of a standardized histopathology scoring system using machine learning algorithms for intervertebral disc degeneration in the mouse model—An ORS spine section initiative. *JOR SPINE* **4**, e1164.

Mir, M. M., Alfaifi, J., Sohail, S. K., Rizvi, S. F., Akhtar, M. T., Alghamdi, M. A. A., Mir, R., Wani, J. I., Sabah, Z. U., Alhumaydhi, F. A., et al. (2024). The Role of Pro-Inflammatory Chemokines CCL-1, 2, 4, and 5 in the Etiopathogenesis of Type 2 Diabetes Mellitus in Subjects from the Asir Region of Saudi Arabia: Correlation with Different Degrees of Obesity. *J. Pers. Med.* **14**, 743.

Molinos, M., Almeida, C. R., Caldeira, J., Cunha, C., Gonçalves, R. M. and Barbosa, M. A. (2015). Inflammation in intervertebral disc degeneration and regeneration. *J. R. Soc. Interface* **12**, 20141191.

Mortara, L., Balza, E., Bruno, A., Poggi, A., Orecchia, P. and Carnemolla, B. (2018). Anti-cancer Therapies Employing IL-2 Cytokine Tumor Targeting: Contribution of Innate, Adaptive and Immunosuppressive Cells in the Anti-tumor Efficacy. *Front. Immunol.* **9**,.

Motwani, M. and Gilroy, D. (2015). Macrophage development and polarization in chronic inflammation. *Semin. Immunol.* **27**,.

Mu, J., Woods, J., Zhou, Y.-P., Roy, R. S., Li, Z., Zycband, E., Feng, Y., Zhu, L., Li, C., Howard, A. D., et al. (2006). Chronic Inhibition of Dipeptidyl Peptidase-4 With a Sitagliptin Analog Preserves Pancreatic β-Cell Mass and Function in a Rodent Model of Type 2 Diabetes. *Diabetes* **55**, 1695–1704.

Mu, J., Petrov, A., Eiermann, G. J., Woods, J., Zhou, Y.-P., Li, Z., Zycband, E., Feng, Y., Zhu, L., Roy, R. S., et al. (2009). Inhibition of DPP-4 with sitagliptin improves glycemic control and restores islet cell mass and function in a rodent model of type 2 diabetes. *Eur. J. Pharmacol.* **623**, 148–154.

National Diabetes Statistics Report | Diabetes | CDC (2022).

Navone, S. E., Marfia, G., Giannoni, A., Beretta, M., Guarnaccia, L., Gualtierotti, R., Nicoli, D., Rampini, P. and Campanella, R. (2017). Inflammatory mediators and signalling pathways controlling intervertebral disc degeneration. *Histol. Histopathol.* 523–542.

Nawaz, M. I., Van Raemdonck, K., Mohammad, G., Kangave, D., Van Damme, J., Abu El-Asrar, A. M. and Struyf, S. (2013). Autocrine CCL2, CXCL4, CXCL9 and CXCL10 signal in retinal endothelial cells and are enhanced in diabetic retinopathy. *Exp. Eye Res.* **109**, 67–76.

Ochiai, E., Sa, Q., Brogli, M., Kudo, T., Wang, X., Dubey, J. P. and Suzuki, Y. (2015). CXCL9 Is Important for Recruiting Immune T Cells into the Brain and Inducing an Accumulation of the T Cells to the Areas of Tachyzoite Proliferation to Prevent Reactivation of Chronic Cerebral Infection with *Toxoplasma gondii*. *Am. J. Pathol.* **185**, 314–324.

Pan, X., Kaminga, A. C., Wen, S. W. and Liu, A. (2021). Chemokines in Prediabetes and Type 2 Diabetes: A Meta-Analysis. *Front. Immunol.* **12**,.

Pelisch, N., Rosas Almanza, J., Stehlik, K. E., Aperi, B. V. and Kroner, A. (2020). CCL3 contributes to secondary damage after spinal cord injury. *J. Neuroinflammation* **17**, 362.

Petersen, M. C. and Shulman, G. I. (2018). Mechanisms of Insulin Action and Insulin Resistance. *Physiol. Rev.* **98**, 2133–2223.

Pettersson, U. S., Waldén, T. B., Carlsson, P.-O., Jansson, L. and Phillipson, M. (2012). Female Mice are Protected against High-Fat Diet Induced Metabolic Syndrome and Increase the Regulatory T Cell Population in Adipose Tissue. *PLOS ONE* **7**, e46057.

Pettigrew, K. A., McKnight, A. J., Patterson, C. C., Kilner, J., Sadlier, D. M. and Maxwell, A. P. (2010). Resequencing of the CCL5 and CCR5 genes and investigation of variants for association with diabetic nephropathy. *J. Hum. Genet.* **55**, 248–251.

Pinto, E. M., Neves, J. R., Laranjeira, M. and Reis, J. (2023). The importance of inflammatory biomarkers in non-specific acute and chronic low back pain: a systematic review. *Eur. Spine J.*

Rebuffat, S. A., Sidot, E., Guzman, C., Azay-Milhau, J., Jover, B., Lajoix, A.-D. and Peraldi-Roux, S. (2018). Adipose tissue derived-factors impaired pancreatic β-cell function in diabetes. *Biochim. Biophys. Acta BBA - Mol. Basis Dis.* **1864**, 3378–3387.

Risbud, M. V. and Shapiro, Irving. M. (2014). Role of Cytokines in Intervertebral Disc Degeneration: Pain and Disc-content. *Nat. Rev. Rheumatol.* **10**, 44–56.

Robinson, D., Mirovsky, Y., Halperin, N., Evron, Z. and Nevo, Z. (1998). Changes in Proteoglycans of Intervertebral Disc in Diabetic Patients: A Possible Cause of Increased Back Pain. *Spine* **23**, 849.

Ruytinx, P., Proost, P., Van Damme, J. and Struyf, S. (2018). Chemokine-Induced Macrophage Polarization in Inflammatory Conditions. *Front. Immunol.* **9**,.

Sagar, D., Lamontagne, A., Foss, C. A., Khan, Z. K., Pomper, M. G. and Jain, P. (2012). Dendritic cell CNS recruitment correlates with disease severity in EAE via CCL2 chemotaxis at the blood–brain barrier through paracellular transmigration and ERK activation. *J. Neuroinflammation* **9**, 245.

Sakaguchi, K., Takeda, K., Maeda, M., Ogawa, W., Sato, T., Okada, S., Ohnishi, Y., Nakajima, H. and Kashiwagi, A. (2015). Glucose area under the curve during oral glucose tolerance test as an index of glucose intolerance. *Diabetol. Int.* **7**, 53–58.

Sakellaridis, N. (2006). The influence of diabetes mellitus on lumbar intervertebral disk herniation. *Surg. Neurol.* **66**, 152–154.

Segar, A. H., Fairbank, J. C. T. and Urban, J. (2019). Leptin and the intervertebral disc: a biochemical link exists between obesity, intervertebral disc degeneration and low back pain—an in vitro study in a bovine model. *Eur. Spine J.* **28**, 214–223.

Shachar, I. and Karin, N. (2013). The dual roles of inflammatory cytokines and chemokines in the regulation of autoimmune diseases and their clinical implications. *J. Leukoc. Biol.* **93**, 51–61.

Sharma, A. (2018). The Role of Adipokines in Intervertebral Disc Degeneration. *Med. Sci.* **6**, 34.

Sheng, D., Ma, W., Zhang, R., Zhou, L., Deng, Q., Tu, J., Chen, W., Zhang, F., Gao, N., Dong, M., et al. (2022). Ccl3 enhances docetaxel chemosensitivity in breast cancer by triggering proinflammatory macrophage polarization. *J. Immunother. Cancer* **10**, e003793.

Sindhu, S., Kochumon, S., Shenouda, S., Wilson, A., Al-Mulla, F. and Ahmad, R. (2019). The Cooperative Induction of CCL4 in Human Monocytic Cells by TNF-α and Palmitate Requires MyD88 and Involves MAPK/NF-κB Signaling Pathways. *Int. J. Mol. Sci.* **20**, 4658.

Srinivasan, K. and Ramarao, P. (2007). Animal models in type 2 diabetes research: An overview. *Indian J. Med. Res.* **125**, 451.

Stott, N. L. and Marino, J. S. (2020). High Fat Rodent Models of Type 2 Diabetes: From Rodent to Human. *Nutrients* **12**, 3650.

Stubbins, R. E., Holcomb, V. B., Hong, J. and Núñez, N. P. (2012). Estrogen modulates abdominal adiposity and protects female mice from obesity and impaired glucose tolerance. *Eur. J. Nutr.* **51**, 861–870.

Suri, S., Mitra, P., Abhilasha, A., Saxena, I., Garg, M. K., Bohra, G. K. and Sharma, P. (2022). Role of interleukin-2 and interleukin-18 in newly diagnosed type 2 diabetes mellitus. *J. Basic Clin. Physiol. Pharmacol.* **33**, 185–190.

Twarda-Clapa, A., Olczak, A., Białkowska, A. M. and Koziołkiewicz, M. (2022). Advanced Glycation End-Products (AGEs): Formation, Chemistry, Classification, Receptors, and Diseases Related to AGEs. *Cells* **11**, 1312.

Venetz, D., Ponzoni, M., Schiraldi, M., Ferreri, A. J. M., Bertoni, F., Doglioni, C. and Uguccioni, M. (2010). Perivascular expression of CXCL9 and CXCL12 in primary central nervous system lymphoma: T-cell infiltration and positioning of malignant B cells. *Int. J. Cancer* **127**, 2300–2312.

Xu, P., Zhang, F., Chang, M., Zhong, C., Sun, C.-H., Zhu, H.-R., Yao, J.-C., Li, Z.-Z., Li, S.-T., Zhang, W.-C., et al. (2021a). Recruitment of γδ T cells to the lesion via the CCL2/CCR2 signaling after spinal cord injury. *J. Neuroinflammation* **18**, 64.

Xu, L., Chen, Y., Nagashimada, M., Ni, Y., Zhuge, F., Chen, G., Li, H., Pan, T., Yamashita, T., Mukaida, N., et al. (2021b). CC chemokine ligand 3 deficiency ameliorates diet-induced steatohepatitis by regulating liver macrophage recruitment and M1/M2 status in mice. *Metabolism* **125**, 154914.

Yang, J., Agarwal, M., Ling, S., Teitz-Tennenbaum, S., Zemans, R. L., Osterholzer, J. J., Sisson, T. H. and Kim, K. K. (2020). Diverse Injury Pathways Induce Alveolar Epithelial Cell CCL2/12, Which Promotes Lung Fibrosis. *Am. J. Respir. Cell Mol. Biol.* **62**, 622–632.

Yin, R., Xue, Y., Hu, J., Hu, X. and Shen, Q. (2020). The effects of diet and streptozotocin on metabolism and gut microbiota in a type 2 diabetes mellitus mouse model. *Food Agric. Immunol.* **31**, 723–739.

Zeng, Z., Lan, T., Wei, Y. and Wei, X. (2022). CCL5/CCR5 axis in human diseases and related treatments. *Genes Dis.* **9**, 12–27.

Zhang, X., Fan, L., Wu, J., Xu, H., Leung, W. Y., Fu, K., Wu, J., Liu, K., Man, K., Yang, X., et al. (2019). Macrophage p38α promotes nutritional steatohepatitis through M1 polarization. *J. Hepatol.* **71**, 163–174.

Figure 1. Experimental design, animal model, and workflow of the current study. (A) The db/db model arises due to a point mutation in the leptin receptor gene, while the STZ-HFD model develops diabetes through a pro-glycemic diet and beta cell impairment. Both models present symptoms of obesity, chronic hyperglycemia, and insulin resistance, though the magnitude can vary both between and within each model. **(B)** The experimental timeline outlines the progression of the study for both models. The db/db mice are acquired at skeletal maturity (12 weeks old) and sacrificed after metabolic measurements are collected. For the STZ-HFD model, mice undergo a lead-in phase of 4-6 weeks on a HFD followed by a single low dose of STZ. Subsequently, the experimental phase for the STZ-HFD mice continues with HFD for 12 weeks, with periodic assessments of fasting blood glucose, A1c levels, and glucose tolerance. **(C)** After sacrifice, FSUs, consisting of the intervertebral disc and the adjacent vertebral bodies, are extracted from mice. FSUs are then utilized for terminal measures pictured above.

Figure 2. Both db/db and STZ-HFD mice represent a characteristically T2D phenotype. (A) AUC GTT shows elevated glucose intolerance in db/db and STZ-HFD mice, with a highly significant difference between Con+Veh and STZ-HFD ($p < 0.0001$). **(B)** Terminal body weights indicate db/db mice are significantly heavier than db/+ and STZ-HFD mice. **(C)** Terminal fasting blood glucose levels are significantly higher in STZ-HFD mice compared to Con+Veh. **(D)** HbA1c levels indicate chronic hyperglycemia in both db/db and STZ-HFD mice, with no difference between them, but significant differences from their respective controls.

784

Figure 3. STZ-HFD mice exhibit more severe histopathological IVD degeneration compared to db/db mice. (A) Comparison of histological phenotypes in db/+, db/db, Con+Veh, and STZ-HFD groups, showing best, median, and worst samples. **(B)** Histopathological scoring shows significantly greater IVD degeneration in STZ-HFD mice versus controls. **(C)** Con+Veh samples have healthy lamellae (▼➡); STZ-HFD samples show degenerate, disorganized lamellae (⇨▽).

Figure 4. Comparative analysis of IVD structure, mechanics, and composition are similar between db/db and STZ-HFD mice. (A)-(C) NPVF, NIDI, and DHI indicate few significant differences in structural integrity between the models. **(D)-(F)** Load slope, energy dissipated, and phase shift demonstrating no significant variations in viscoelastic mechanical behavior. **(G)-(I)** Biochemical content measurements, including collagen, s-GAG, and AGEs, show no significant differences.

Figure 5. STZ-HFD IVD Produces a More Pro-Inflammatory Microenvironment than the db/db IVD in Comparative Analysis of Cytokine Expression. (A) The STZ-HFD model shows a significantly higher fold increase for eight cytokines: CXCL2, CCL2, CCL3, CCL4, CCL12 (monocyte/macrophage associated), IL-2, CXCL9 (T-cell associated), and CCL5 (pleiotropic). **(B)** The STZ-HFD model encompasses a broader and more pronounced cytokine response compared to the db/db model, highlighting the extensive upregulation of inflammatory cytokines in the STZ-HFD model.

Figure 6. STZ-HFD IVD Invokes Unique Inflammatory Signaling Pathways in Networks of Cytokine Expression. (A) The STZ-HFD model shows a distinct network structure, demonstrating the unique upregulation of various inflammatory pathways **(B)** The STZ-HFD and db/db networks each rely on a number of unique (red/blue) and shared (purple) cytokines, indicating both leptin-dependent and leptin-independent inflammatory signaling cascades **(C)** The STZ-HFD mouse model displays a fragmented and modular cytokine network, indicating the parallel signaling of multiple signaling pathways.

Figure 7. Enhanced Pathway Disruption in the STZHFD Model Highlights the Complexity of T2D Pathophysiology in the IVD (A) The STZHFD (marked with 2) model exhibits greater transcriptional alterations in T2D-related pathways than db/db (marked with 1) model, particularly in non-enzymatic glycosylation and RAGE signaling. **(B)** Immune response and inflammation pathways, including ubiquitination and proteasome degradation, are significantly disrupted in the STZHFD model but remain unaltered in db/db. **(C)** ECM remodelingd structural integrity pathways are more extensively downregulated in the STZHFD model, suggesting greater tissue disruption. **(D)** Metabolic dysfunction is more pronounced in the STZHFD model, with additional upregulation of pathways involved in amino acid metabolism and gluconeogenesis. **(E)** Signal transduction and tissue differentiation pathways show significant alterations in the STZHFD model, indicating complex changes in cellular communication and development processes.

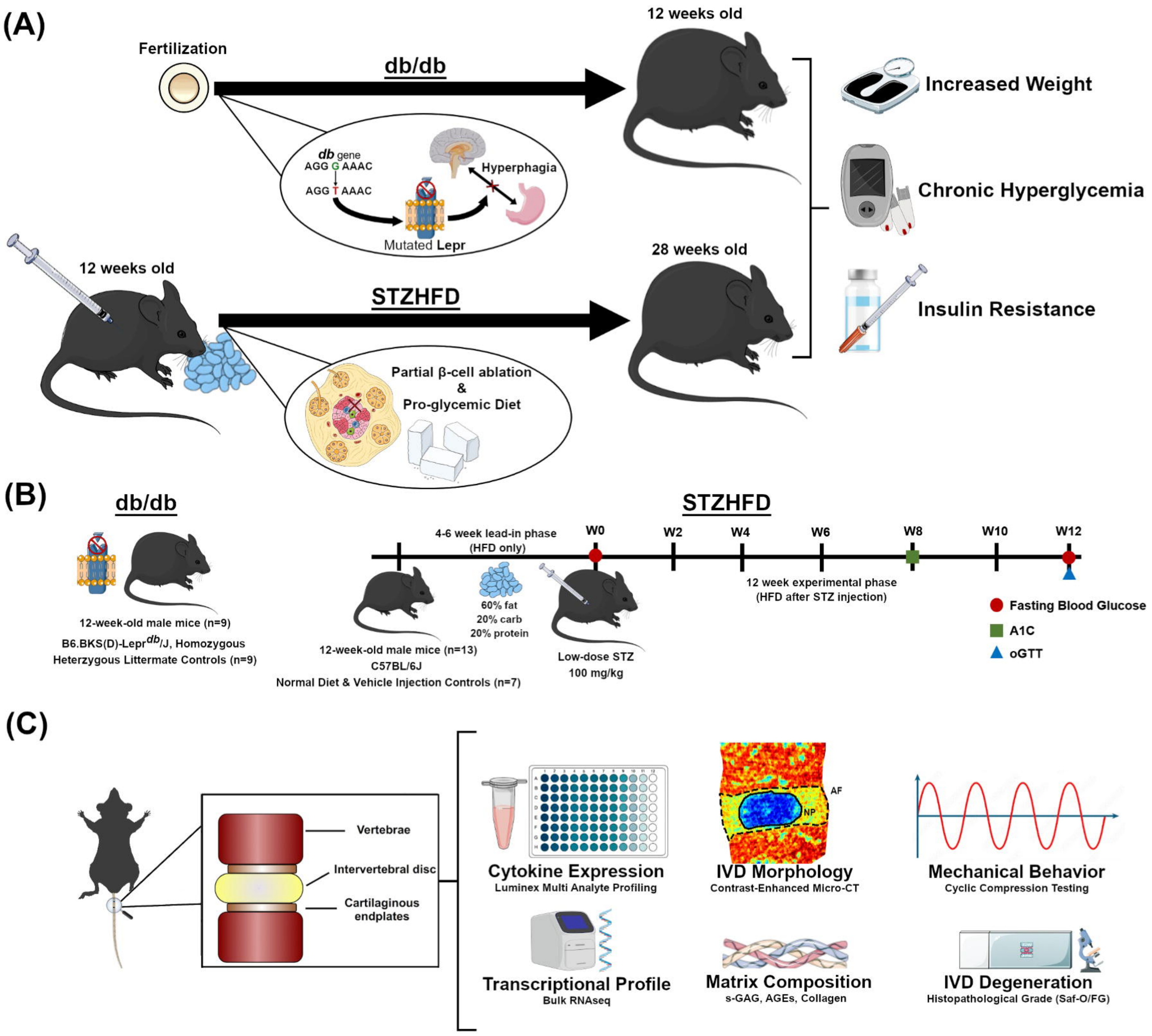
(A)
Fertilization
db/db
12 weeks old
db gene
AGG G AAAC
AGG T AAAC
Hyperphagia
Mutated Lepr
Increased Weight
Chronic Hyperglycemia
Insulin Resistance
12 weeks old
STZHFD
28 weeks old
Partial β-cell ablation
&
Pro-glycemic Diet
(B)
db/db
STZHFD
4-6 week lead-in phase
(HFD only)
W0
W2
W4
W6
W8
W10
W12
12-week-old male mice (n=9)
B6.BKS(D)-Lepr^{db}/J, Homozygous
Heterzygous Littermate Controls (n=9)
60% fat
20% carb
20% protein
12-week-old male mice (n=13)
C57BL/6J
Normal Diet & Vehicle Injection Controls (n=7)
Low-dose STZ
100 mg/kg
12 week experimental phase
(HFD after STZ injection)
Fasting Blood Glucose
A1C
oGTT
(C)
Vertebrae
Intervertebral disc
Cartilaginous endplates
Cytokine Expression
Luminex Multi Analyte Profiling
AF
NP
IVD Morphology
Contrast-Enhanced Micro-CT
Mechanical Behavior
Cyclic Compression Testing
Transcriptional Profile
Bulk RNAseq
Matrix Composition
s-GAG, AGEs, Collagen
IVD Degeneration
Histopathological Grade (Saf-O/FG)

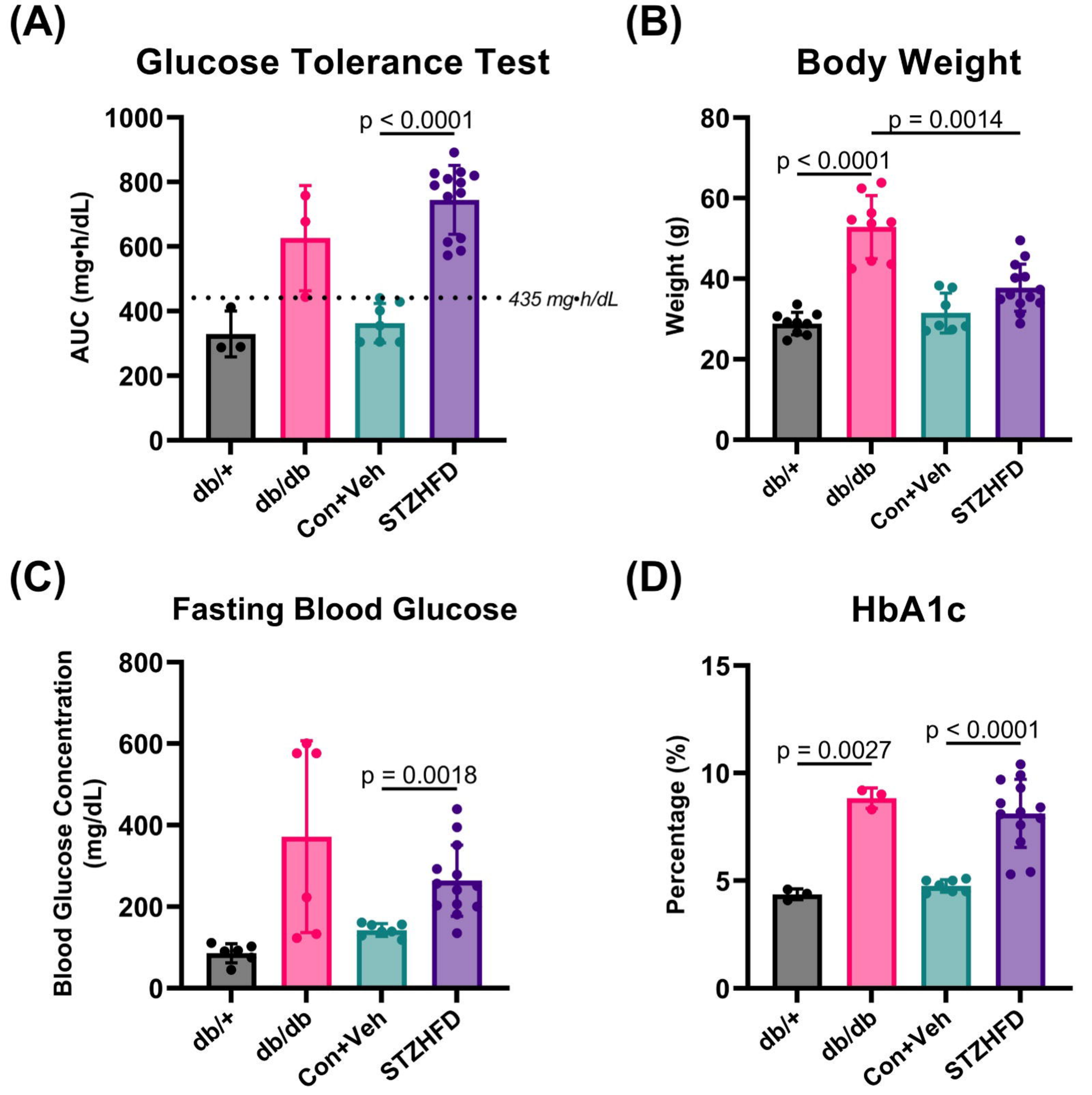
(A)
Glucose Tolerance Test
AUC (mg•h/dL)
1000
800
600
400
200
0
p < 0.0001
435 mg•h/dL
db/+
db/db
Con+Veh
STZHFD
(B)
Body Weight
Weight (g)
80
60
40
20
0
p = 0.0014
p < 0.0001
db/+
db/db
Con+Veh
STZHFD
(C)
Fasting Blood Glucose
Blood Glucose Concentration (mg/dL)
800
600
400
200
0
p = 0.0018
db/+
db/db
Con+Veh
STZHFD
(D)
HbA1c
Percentage (%)
15
10
5
0
p = 0.0027
p < 0.0001
db/+
db/db
Con+Veh
STZHFD

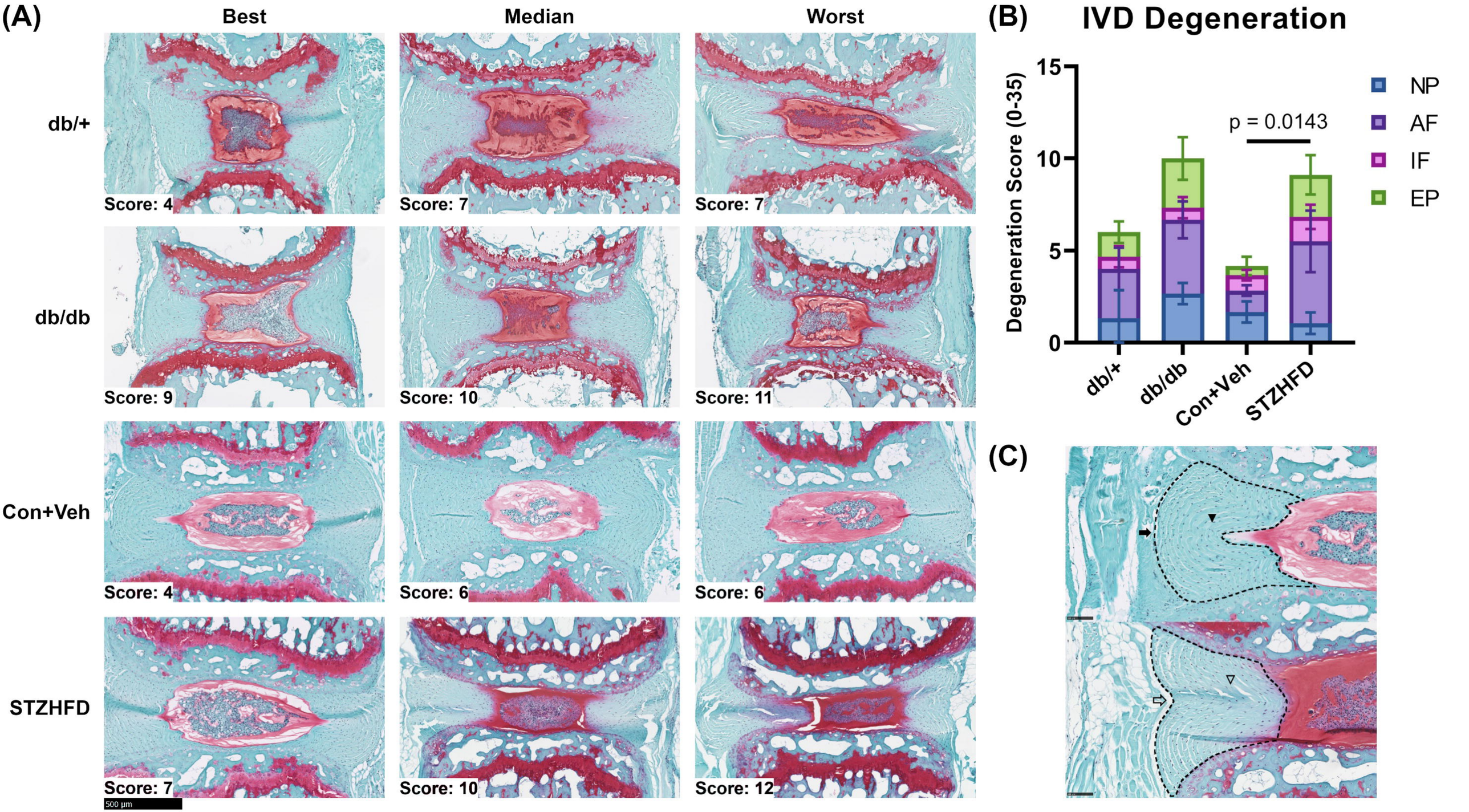
(A)
Best
Median
Worst
db/+
db/db
Con+Veh
STZHFD
Score: 4
Score: 7
Score: 7
Score: 9
Score: 10
Score: 11
Score: 4
Score: 6
Score: 6
Score: 7
Score: 10
Score: 12
500 µm
(B)
IVD Degeneration
Degeneration Score (0-35)
15
10
5
0
p = 0.0143
NP
AF
IF
EP
db/+
db/db
Con+Veh
STZHFD
(C)

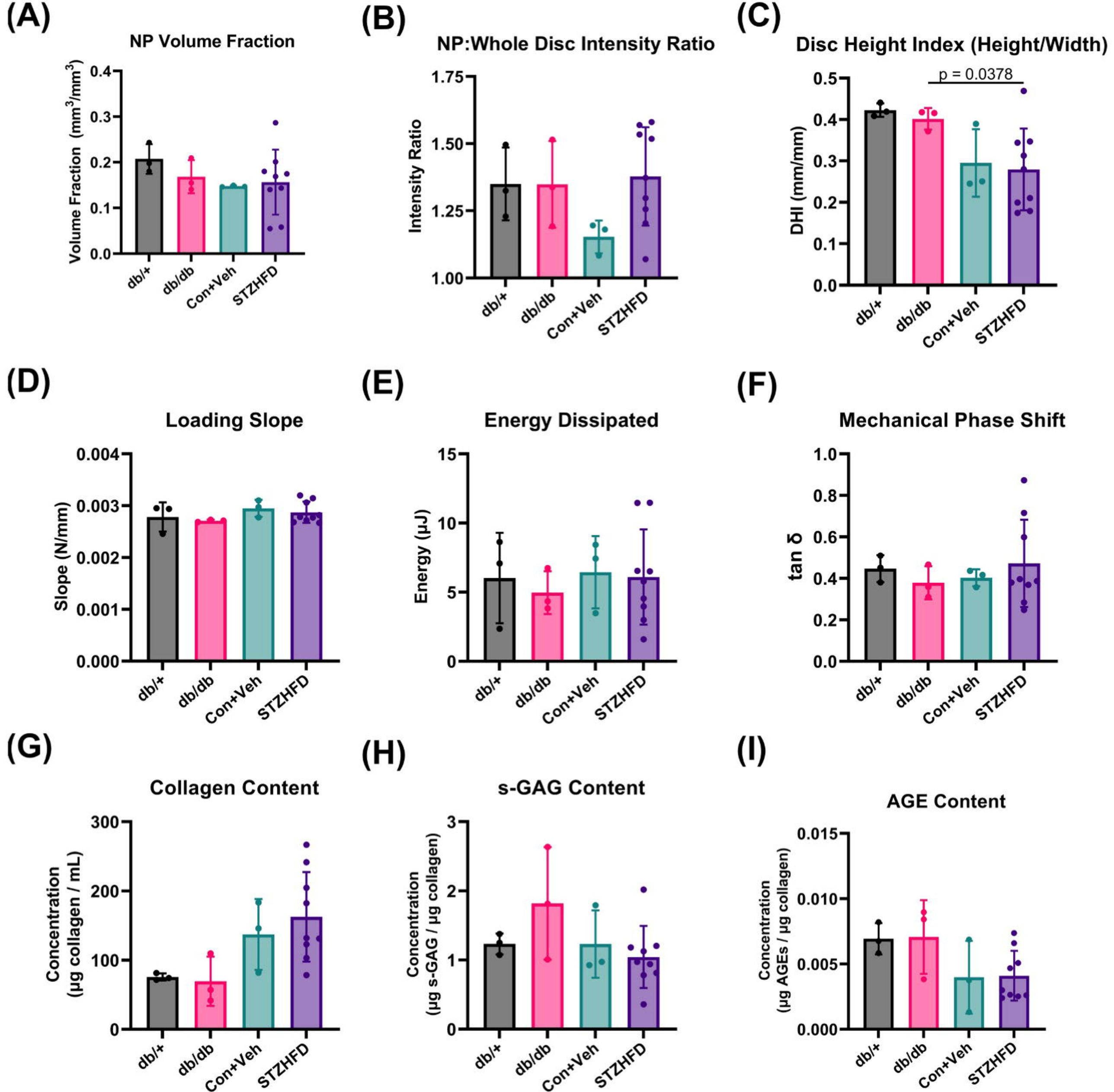
(A)
NP Volume Fraction
Volume Fraction (mm3/mm3)
0.0
0.1
0.2
0.3
0.4
db/+
db/db
Con+Veh
STZHFD
(B)
NP:Whole Disc Intensity Ratio
Intensity Ratio
1.00
1.25
1.50
1.75
db/+
db/db
Con+Veh
STZHFD
(C)
Disc Height Index (Height/Width)
p = 0.0378
DHI (mm/mm)
0.0
0.1
0.2
0.3
0.4
0.5
db/+
db/db
Con+Veh
STZHFD
(D)
Loading Slope
Slope (N/mm)
0.000
0.001
0.002
0.003
0.004
db/+
db/db
Con+Veh
STZHFD
(E)
Energy Dissipated
Energy (μJ)
0
5
10
15
db/+
db/db
Con+Veh
STZHFD
(F)
Mechanical Phase Shift
tan δ
0.0
0.2
0.4
0.6
0.8
1.0
db/+
db/db
Con+Veh
STZHFD
(G)
Collagen Content
Concentration (μg collagen / mL)
0
100
200
300
db/+
db/db
Con+Veh
STZHFD
(H)
s-GAG Content
Concentration (μg s-GAG / μg collagen)
0
1
2
3
db/+
db/db
Con+Veh
STZHFD
(I)
AGE Content
Concentration (μg AGEs / μg collagen)
0.000
0.005
0.010
0.015
db/+
db/db
Con+Veh
STZHFD

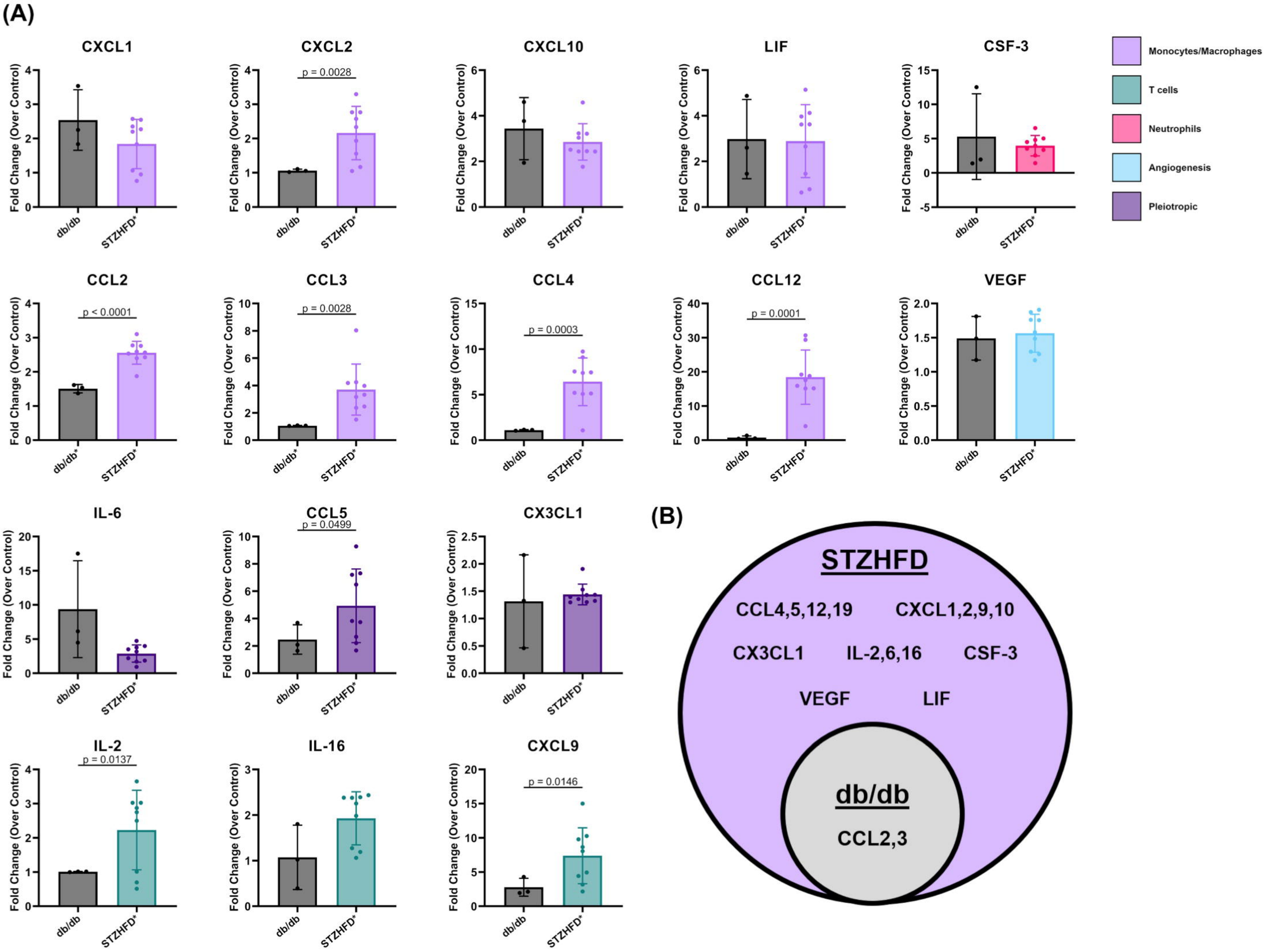
(A)
CXCL1
CXCL2
p = 0.0028
CXCL10
LIF
CSF-3
CCL2
p < 0.0001
CCL3
p = 0.0028
CCL4
p = 0.0003
CCL12
p = 0.0001
VEGF
IL-6
CCL5
p = 0.0499
CX3CL1
IL-2
p = 0.0137
IL-16
CXCL9
p = 0.0146
Fold Change (Over Control)
db/db
db/db*
STZHFD*
Monocytes/Macrophages
T cells
Neutrophils
Angiogenesis
Pleiotropic
(B)
STZHFD
CCL4,5,12,19
CXCL1,2,9,10
CX3CL1
IL-2,6,16
CSF-3
VEGF
LIF
db/db
CCL2,3

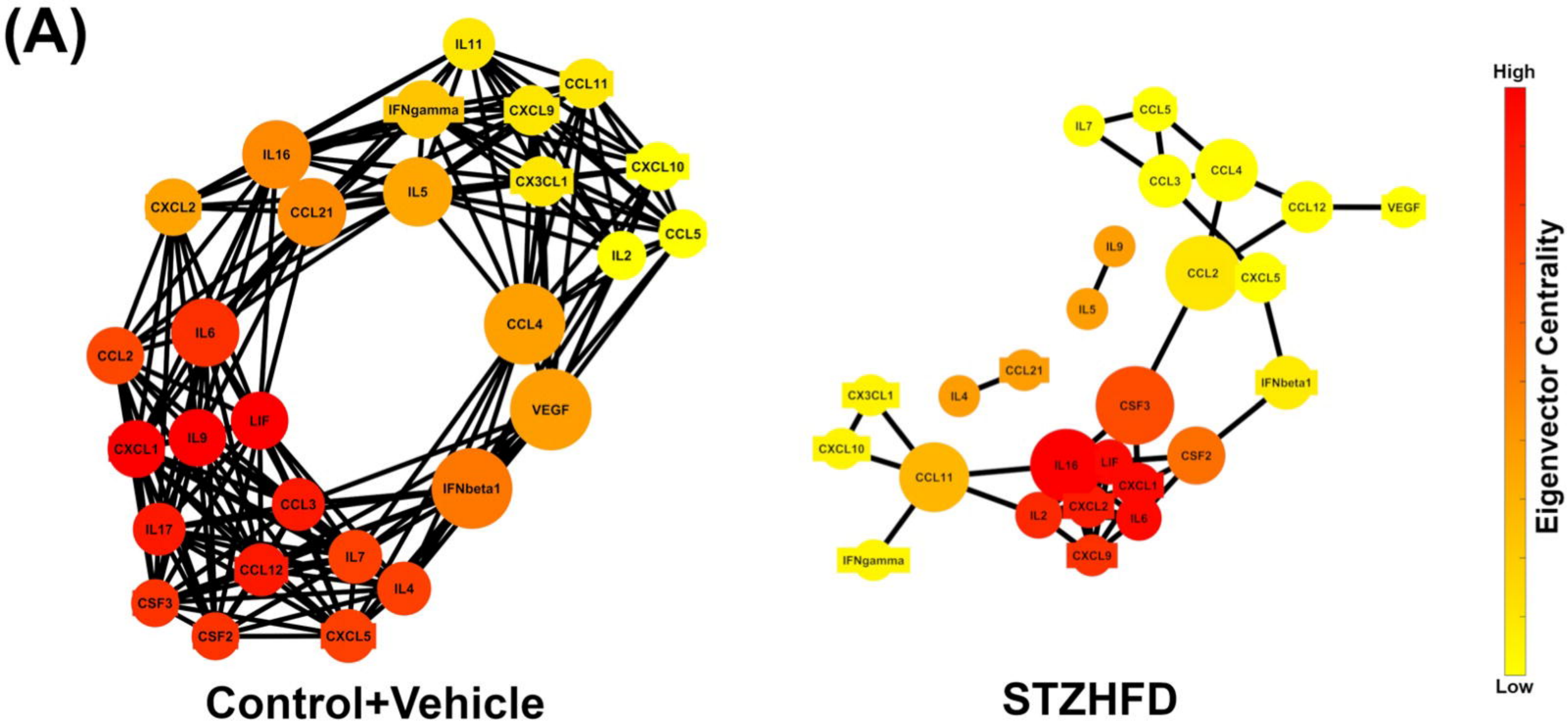

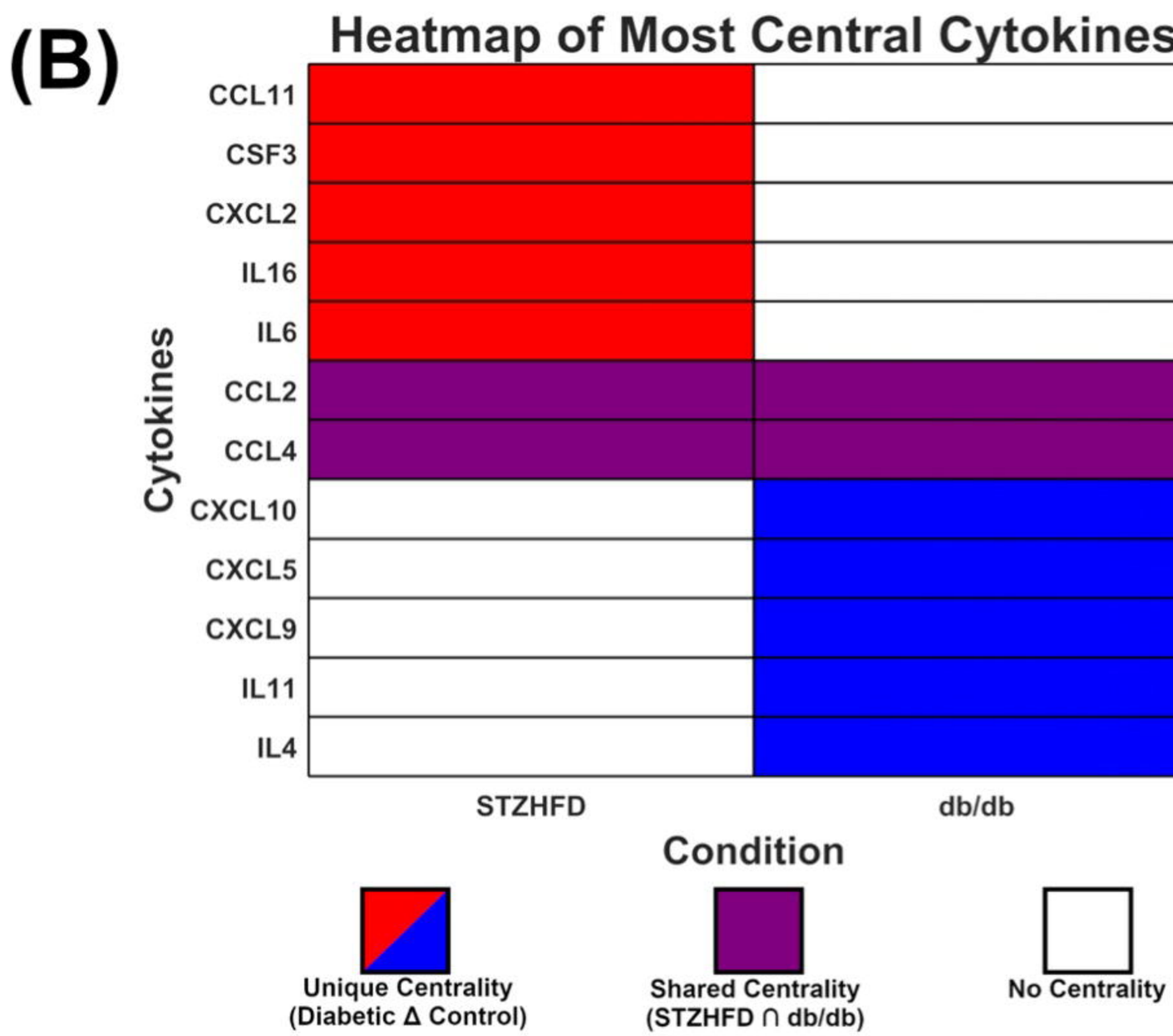

(C)

Metric	Con+Veh	STZHFD	db/+	db/db
Path Length	1.3	2.3	1.3	1.3
Modularity	0.34	0.45	0.29	0.18
	Con+Veh vs STZHFD	db/db vs STZHFD	db/+ vs db/db	db/+ vs Con+Veh
Jaccard Index (k=1)	0.14	0.13	0.21	0.15
Jaccard Index (k=2)	0.25	0.24	0.37	0.32

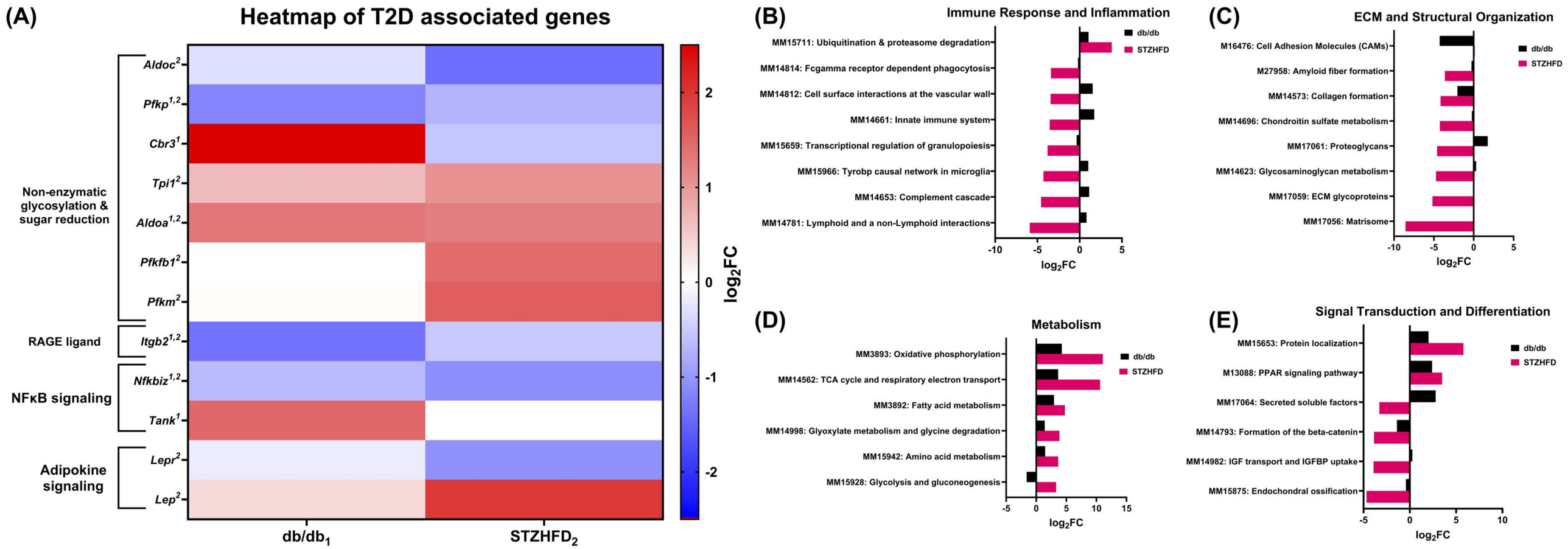
(A)
Heatmap of T2D associated genes
Aldoc2
Pfkp1,2
Cbr31
Tpi12
Aldoa1,2
Pfkfb12
Pfkm2
Itgb21,2
Nfkbiz1,2
Tank1
Lepr2
Lep2
Non-enzymatic glycosylation & sugar reduction
RAGE ligand
NFκB signaling
Adipokine signaling
db/db1
STZHFD2
log2FC
2
1
0
-1
-2
(B)
Immune Response and Inflammation
MM15711: Ubiquitination & proteasome degradation
MM14814: Fcgamma receptor dependent phagocytosis
MM14812: Cell surface interactions at the vascular wall
MM14661: Innate immune system
MM15659: Transcriptional regulation of granulopoiesis
MM15966: Tyrobp causal network in microglia
MM14653: Complement cascade
MM14781: Lymphoid and a non-Lymphoid interactions
db/db
STZHFD
-10
-5
0
5
log2FC
(C)
ECM and Structural Organization
M16476: Cell Adhesion Molecules (CAMs)
M27958: Amyloid fiber formation
MM14573: Collagen formation
MM14696: Chondroitin sulfate metabolism
MM17061: Proteoglycans
MM14623: Glycosaminoglycan metabolism
MM17059: ECM glycoproteins
MM17056: Matrisome
db/db
STZHFD
-10
-5
0
5
log2FC
(D)
Metabolism
MM3893: Oxidative phosphorylation
MM14562: TCA cycle and respiratory electron transport
MM3892: Fatty acid metabolism
MM14998: Glyoxylate metabolism and glycine degradation
MM15942: Amino acid metabolism
MM15928: Glycolysis and gluconeogenesis
db/db
STZHFD
-5
0
5
10
15
log2FC
(E)
Signal Transduction and Differentiation
MM15653: Protein localization
M13088: PPAR signaling pathway
MM17064: Secreted soluble factors
MM14793: Formation of the beta-catenin
MM14982: IGF transport and IGFBP uptake
MM15875: Endochondral ossification
db/db
STZHFD
-5
0
5
10
log2FC